A&A 424, 647–655 (2004)
DOI: 10.1051/0004-6361:20040408

Astronomy & Astrophysics

Time-resolved photometry and spectroscopy of the new deeply-eclipsing SW Sextantis star HS 0728+6738⋆

P. Rodríguez-Gil[1], B. T. Gänsicke[1], H. Barwig[2], H.-J. Hagen[3], and D. Engels[3]

[1] Department of Physics, University of Warwick, Coventry CV4 7AL, UK
e-mail: Pablo.Rodriguez-Gil@warwick.ac.uk
[2] Universitäts-Sternwarte, Scheinerstr. 1, 81679 München, Germany
[3] Hamburger Sternwarte, Universität Hamburg, Gojenbergsweg 112, 21029 Hamburg, Germany

Received 8 March 2004 / Accepted 28 May 2004

Abstract. We present time-resolved optical spectroscopy and photometry, and far-ultraviolet spectroscopy of HS 0728+6738, a cataclysmic variable discovered in the Hamburg Quasar Survey. We show that the system is a new eclipsing member of the SW Sex class of CVs with an orbital period of 3.21 h. We derive an orbital inclination of $\sim 85 \pm 4°$ from the average eclipse profile, making HS 0728+6738 the highest inclination SW Sex star known. The optical and far-ultraviolet emission lines are not or only weakly occulted during the eclipse, indicating the presence of line-emission sites either far outside the Roche lobe of the primary or, more likely, above the orbital plane of the binary. The photometric light curves exhibit fast variability with a period of ∼7 min, which might be related to the spin of the white dwarf.

Key words. accretion, accretion disks – stars: binaries: close – stars: individual: HS 0728+6738 – stars: novae, cataclysmic variables

1. Introduction

The SW Sextantis stars compose a group of nova-like (NL) cataclysmic variables (CVs). The NLs lack the characteristic eruptive behaviour shown by their dwarf novae cousins (see Warner 1995 for a general review on NLs and CVs in general). The SW Sex stars display a number of so far poorly understood characteristics, most noticeably a very complex behaviour of their emission lines (Thorstensen et al. 1991). More recently, Rodríguez-Gil et al. (2001a, see also Rodríguez-Gil 2003) and Hameury & Lasota (2002) independently suggested that the SW Sex stars may contain magnetic white dwarfs. Rodríguez-Gil et al. (2001a) also pointed out the possibility of these systems being intermediate polar CVs (IPs; CVs with magnetically truncated discs and asynchronously rotating primaries) with the highest mass transfer rates.

The combination of the exotic but consistent behaviour of the known SW Sex stars and their strong clustering in the 3–4 h orbital period range may very well be an important clue for a global understanding of CV evolution. Nevertheless, some NLs above the 3–4 h period interval are found to exhibit some of the defining features of the SW Sex stars, like BT Mon (Smith et al. 1998) and, more recently, RW Tri (Groot et al. 2004). Beyond the realm of CVs, some Low Mass X-ray Binaries (LMXBs) may show distinctive SW Sex behaviour, such as e.g. XTE J2123–058 (Hynes et al. 2001).

Despite being intrinsically luminous, most SW Sex stars are rather inconspicuous, displaying no outbursts and being weak X-ray emitters. In fact, about one third of the currently known SW Sex stars have been discovered as fairly bright blue objects in the Palomar-Green survey (Green et al. 1986).

We are currently carrying out a large-scale search for CVs based on the spectroscopic hallmark of most of them: the presence of strong emission lines in their spectra (Gänsicke et al. 2002b). Among the CVs followed up in more detail (e.g. Gänsicke et al. 2000; Nogami et al. 2000; Araujo-Betancor et al. 2003; Rodríguez-Gil et al. 2004; Gänsicke et al. 2004), our survey has so far produced two new SW Sextantis stars (Szkody et al. 2001; Gänsicke et al. 2002c). Here we report

⋆ Based in part on observations obtained at the German-Spanish Astronomical Center, Calar Alto, operated by the Max-Planck-Institut für Astronomie, Heidelberg, jointly with the Spanish National Commission for Astronomy, on observations made with the IAC80 telescope, operated on the island of Tenerife by the Instituto de Astrofísica de Canarias (IAC) at the Spanish Observatorio del Teide, on observations made at the Wendelstein Observatory, operated by the Universitäts-Sternwarte München, and on observations made with the NASA/ESA Hubble Space Telescope, obtained at the Space Telescope Science Institute, which is operated by the Association of Universities for Research in Astronomy, Inc., under NASA contract NAS 5-26555.

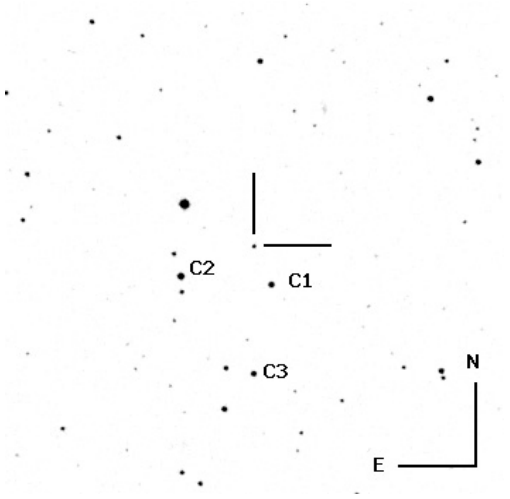

Fig. 1. $10' \times 10'$ finding chart of HS 0728+6738 obtained from the Digitized Sky Survey 2. The coordinates of the CV are α(J2000) = $07^h33^m41.4^s$, δ(J2000) = $+67°32'16.2''$. C1 has been used as primary comparison star for both the Wendelstein *B*-band and IAC80 white-light CCD photometry.

the discovery of a third new and deeply eclipsing member of the class: HS 0728+6738.

2. Observations and data reduction

2.1. Photometry

Differential CCD photometry of HS 0728+6738 was obtained during 11 nights in the period April to June 2001 with the 0.8-m telescope at Wendelstein Observatory, Germany, and during 3 nights on 2003 September 24, 25 and 27 with the 0.82-m IAC80 telescope at the Observatorio del Teide on Tenerife, Spain (Table 1). At Wendelstein we used the MONICA CCD camera (Roth 1992) which is equipped with a 1024×1024 pixel^2 TeK CCD detector. All the images were taken through a broadband Bessel *B* filter. Standard bias subtraction and flat-field correction were done in MIDAS, and aperture photometry was performed using the SEXTRACTOR (Bertin & Arnouts 1996). A more detailed account of the employed photometry reduction pipeline is given by Gänsicke et al. (2004). The instrumental magnitudes of HS 0728+6738 were derived relative to the comparison star "C1" (Fig. 1), whilst "C2" and "C3" were used as secondary comparison stars during different nights.

The white-light observations of HS 0728+6738 at the IAC80 telescope were performed with the Thomson 1024×1024 pixel^2 CCD camera using an exposure time of 20 s. We only read out a small window on the CCD to improve the time resolution which was always better than 30 s. The individual images were bias-corrected and then flat-fielded in the usual way. All the data reduction was done with the IRAF[1] package. The instrumental magnitudes of the target and three comparison stars were then calculated using Point Spread Function (PSF) photometry, and differential light curves were constructed relative to comparison star "C1" (Fig. 1). Full details of the observations are given in Table 1.

[1] IRAF is distributed by the National Optical Astronomy Observatories, which is operated by the Association of Universities for Research in Astronomy, Inc., under contract with the National Science Foundation.

Table 1. Log of observations.

Date	Coverage (h)	Filter/Grating	Exp. (s)	Frames
Calar Alto 3.5 m, TWIN spectroscopy				
2002 Dec. 02	1.73	T05/T06	600	10
2002 Dec. 03	8.51	T05/T06	600	23
2002 Dec. 04	1.87	T05/T06	600	12
Hubble Space Telescope 2.4 m, STIS spectroscopy				
2003 Mar. 19		G140L	730	1
Wendelstein 0.8 m, CCD photometry				
2001 Apr. 01	4.19	*B*	240	56
2001 Apr. 23	2.79	*B*	240	38
2001 Apr. 24	4.63	*B*	60	109
2001 Apr. 26	1.56	*B*	120	39
2001 Apr. 29	1.16	*B*	60	40
2001 May 01	1.44	*B*	60	55
2001 May 02	4.08	*B*	60	141
2001 May 04	4.06	*B*	60	161
2001 May 09	1.32	*B*	60	47
2001 May 26	1.03	*B*	60	31
2001 Jun. 07	1.17	*B*	60	63
IAC80 0.8 m, CCD photometry				
2003 Sep. 24	1.35	White light	20	156
2003 Sep. 25	2.64	White light	20	330
2003 Sep. 27	1.49	White light	20	182

2.2. Optical spectroscopy

Time-resolved spectroscopy of HS 0728+6738 was performed on 2002 December 2, 3 and 4 with the 3.5-m telescope at Calar Alto Observatory (Almería, Spain). The standard SITe 2000×800 pixel^2 detectors of the TWIN spectrograph were used to simultaneously image blue and red spectra (gratings T05 and T06, respectively) at a resolution of 1.2 Å (*FWHM*; 1.5″ slit width). The sampled wavelength ranges were $\lambda\lambda$3810–4940 and $\lambda\lambda$6440–7510 in the blue and red arms, respectively. A comparison spectrum of a He–Ar lamp was acquired every three target exposures to guarantee an accurate wavelength calibration. A log of the spectroscopic observations can be found in Table 1.

The raw images were corrected for the effects of bias and flat-field structure and then sky-subtracted. The target spectra were optimally extracted using the algorithm of Horne (1986). For wavelength calibration a low-order polynomial was fitted to the arc data, the rms being always $\lesssim$0.05 Å. The pixel-wavelength relation for each target spectrum was obtained by interpolating between the two nearest arc spectra. These reduction tasks were done with the standard packages for long-slit spectra within IRAF. Prior to further analysis the spectra were normalised by using a low-order polynomial fit to the continuum.

Table 2. Eclipse timings.

Time of mid-eclipse (HJD - 2 452 000)	Cycle E	O−C (s)	σ(O−C) (s)
1.3275 ± 0.0003	0	17.3	26.0
1.4612 ± 0.0003	1	24.2	26.0
23.5081 ± 0.0001	166	–2.6	9.0
24.4436 ± 0.0003	173	11.5	26.0
26.3146 ± 0.0001	187	39.8	9.0
26.4478 ± 0.0001	188	3.6	9.0
29.3867 ± 0.0001	210	–59.3	9.0
32.3269 ± 0.0001	232	–9.9	9.0
32.4609 ± 0.0001	233	23.0	9.0
34.4650 ± 0.0001	248	6.4	9.0
39.4087 ± 0.0001	285	–12.6	9.0
56.3786 ± 0.0001	412	7.1	9.0
908.7371 ± 0.0001	6791	4.1	11.0
910.7413 ± 0.0001	6806	–3.9	11.0

2.3. Far-ultraviolet spectroscopy

A brief *Hubble Space Telescope*/Space Telescope Imaging Spectrograph (*HST*/STIS) snapshot observation of HS 0728+6738 was obtained on 2003 March 19 as part of a far-ultraviolet (FUV) spectroscopic survey of CVs (Gänsicke et al. 2003). We used the G140L grating and the $52'' \times 0.2''$ aperture, covering the wavelength range $\lambda\lambda$1150−1710 at a spectral resolution of $R \approx 1000$. The data were reduced with the CALSTIS (V2.13b) pipeline.

3. The light curve of HS 0728+6738

3.1. The orbital period

The first light curve of HS 0728+6738 immediately revealed the presence of deep eclipses during which the brightness of the CV drops by ∼2.5 mag. The observation of two consecutive eclipses during the first night provided an estimate of the orbital period of ∼3.2 h.

A precise long-term ephemeris of HS 0728+6738 was computed using a total of 14 mid-eclipse times measured in the Wendelstein and IAC80 light curves (Table 2). The eclipse timings were measured by fitting parabolas to the bottom part of the eclipses. We have to stress the fact that a number of Wendelstein light curves lack data at the very eclipse centre. The errors given in Table 2 are purely of statistical nature, the true error on the eclipse timings may be larger because of the asymmetry in the wings of the eclipse profiles. A linear least-square fit to the 14 eclipse timings provides the following ephemeris for HS 0728+6738:

$$T_0(\mathrm{HJD}) = 2\,452\,001.32730(3) + 0.13361946(1)\,E. \quad (1)$$

The observed minus calculated (O−C) diagram is shown in Fig. 2. The point with the largest O−C value corresponds indeed to one of the Wendelstein light curves with poor sampling of the eclipse centre. Our current data is consistent with a linear ephemeris.

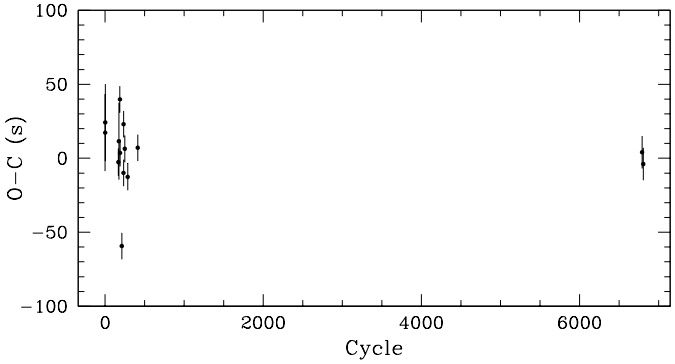

Fig. 2. O−C diagram of the eclipse timings. The errors have been determined by propagating the errors in the measurement of the mid-eclipse times and the corresponding error from the ephemeris.

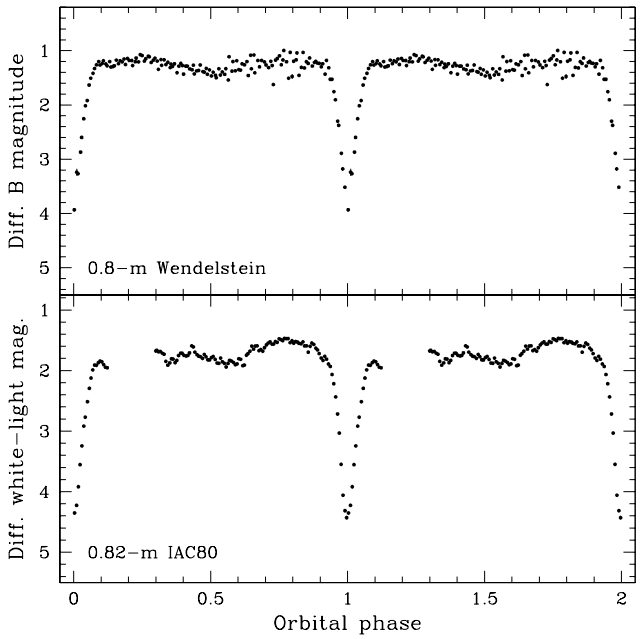

Fig. 3. Average light curves of HS 0728+6738. The individual data points were averaged into 150 phase bins. A full orbital cycle has been plotted twice.

3.2. Light curve morphology

The average Wendelstein (*B* band) and IAC80 (white light) light curves are shown in Fig. 3. Orbital phases were calculated according to the ephemeris given in Eq. (1) and the data were averaged into 150 phase bins. The average eclipse depth in both *B*-band and white light is ∼2.7 mag, probably indicating a high orbital inclination. The eclipse lasts for ∼0.2 orbital cycles, or ∼40 min.

HS 0728+6738 shows also significant short-term variability on a time scale of ≃7−10 min, best resolved in the out-of-eclipse light curve obtained with the IAC80 telescope (Fig. 4). Important information on the origin of this variability could be obtained by studying the phase dependence of its amplitude. In order to check if the oscillation is present during eclipse we subtracted a Gaussian fit to the average eclipse profile in white light from the eclipse profile observed on 2003 September 25 (IAC80 telescope). This eclipse-subtracted light curve was then

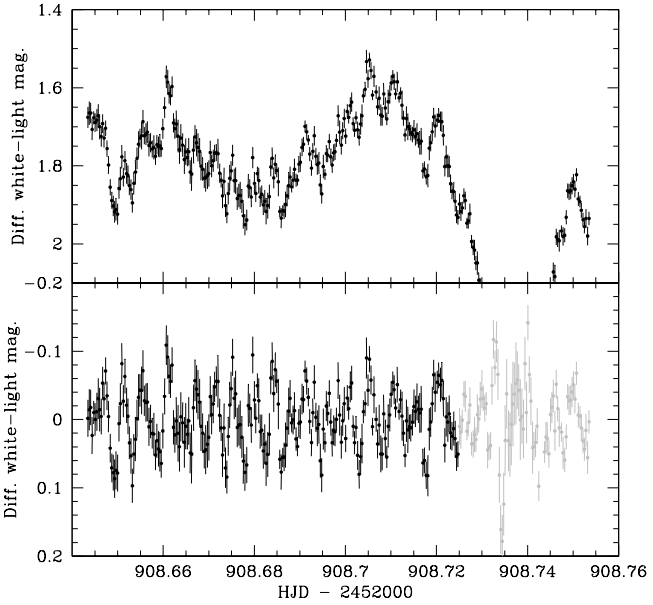

Fig. 4. *Top panel*: out-of-eclipse variability on the 2003 September 25 light curve (IAC80 telescope). A short-period oscillation with a time scale of 7−10 min is easily spotted. *Bottom panel*: same light curve detrended for period analysis. The points plotted in grey lie in the orbital phase interval 0.9−1.1. See text for details.

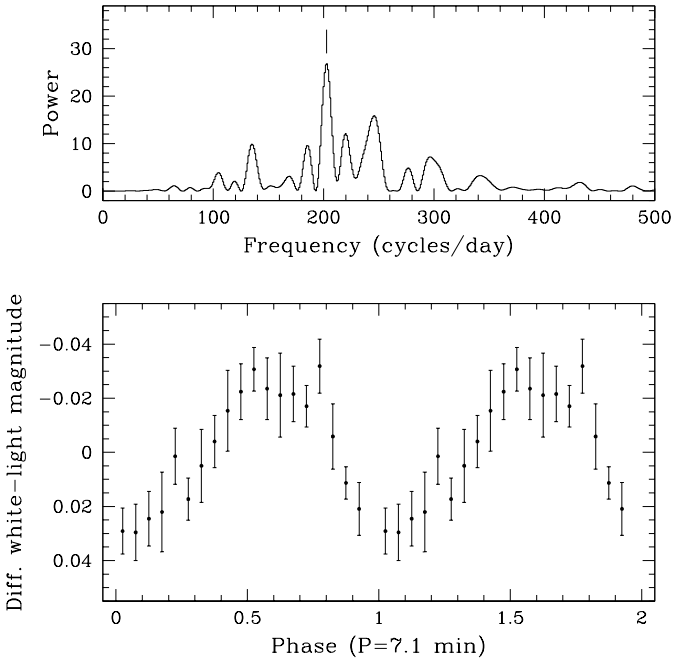

Fig. 5. *Top panel*: Scargle periodogram of the 2003 September 25 light curve (IAC80 telescope) after eliminating the eclipse and detrending. The strongest peak is centred at 7.1 min. *Bottom panel*: the light curve folded on the 7.1-min period after averaging the data into 20 phase bins (the average value has been subtracted). A complete cycle has been repeated for continuity.

detrended by subtracting the same data set smoothed with a 15-point boxcar. The oscillation is clearly present up to $\varphi \sim 0.96$ and again from $\varphi \sim 0.06$ on. It is difficult to say whether it remains during eclipse or not. The spikes that appear during eclipse could be the residuals of the average eclipse profile subtraction, as the average profile is made up of only two eclipses. A larger set of well-sampled light curves is necessary to address any firm conclusion.

In order to analyse this short time scale variability we decided to eliminate the eclipse data. A Scargle periodogram (Scargle 1982) computed from the detrended data is shown in the top panel of Fig. 5. The strongest peak is centred at a period of 7.1 min, confirming the estimate done by eye. Folding the detrended data on this period results in a clear quasi-sinusoidal modulation (see bottom panel of Fig. 5). We will discuss the possible origin of this short-term variation in Sect. 5.2.

3.3. Estimate of the orbital inclination

From the geometry of a point eclipse by a spherical body, it is possible to determine the inclination, i, of a binary system through the relation

$$\left(\frac{R_2}{a}\right)^2 = \sin^2(\pi\Delta\varphi_{1/2}) + \cos^2(\pi\Delta\varphi_{1/2})\cos^2 i, \quad (2)$$

where R_2/a is the volume radius of the secondary star, which depends only on the mass ratio, $q = M_2/M_1$ (Eggleton 1983):

$$\frac{R_2}{a} = \frac{0.49\, q^{2/3}}{0.6\, q^{2/3} + \ln(1 + q^{1/3})}. \quad (3)$$

$\Delta\varphi_{1/2}$ is the mean phase full-width of the eclipse at half the out-of-eclipse intensity. We calculated $\Delta\varphi_{1/2}$ from the B-band average light curve (top panel of Fig. 3), assuming an average out-of-eclipse differential magnitude of ∼1.2. The derived value is $\Delta\varphi_{1/2} = 0.092 \pm 0.002$.

By elimination of R_2/a from Eqs. (2) and (3) we can obtain an estimate of the orbital inclination of the system after assuming a value for the mass ratio, q. Using as an approximation the mass-period relation derived by Smith & Dhillon (1998):

$$M_2(M_\odot) = 0.126\, P_{\rm orb}(\mathrm{h}) - 0.11, \quad (4)$$

where $P_{\rm orb}$(h) is the orbital period expressed in hours, we obtain a value of $M_2 \sim 0.3\ M_\odot$ for the secondary in HS 0728+6738. According to Gänsicke (1997) and Smith & Dhillon (1998), the average mass for primaries in CVs above the gap is $M_1 \sim 0.8\ M_\odot$. In order to provide an estimate of the uncertainty for the orbital inclination, we will assume that the true primary mass lies in the range 0.6−1.0 $M_\odot$. Taking this into account we obtain an orbital inclination of $i = 85 \pm 4°$. Additional systematic uncertainties come from the used $M_2 - P_{\rm orb}$ relation (Eq. (4)) and from the assumption of an axially symmetric accretion disc. The statistical error in the measurement of $\Delta\varphi_{1/2}$ is then negligible.

As we will show in Sect. 5, HS 0728+6738 is a new SW Sex star, and we can hence use the $i - \Delta V$ relation of Rodríguez-Gil et al. (2000) to derive an independent estimate of the orbital inclination. We will assume that the eclipse depth in the V-band does not significantly differ from that in B-band. This assumption is coroborated by the roughly equal depth of the average Wendelstein B-band and the IAC80 white light eclipses.

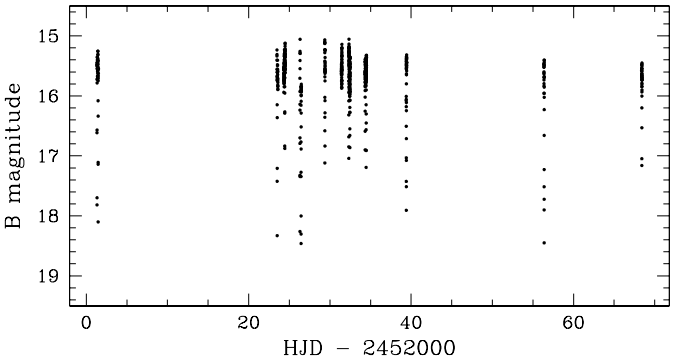

Fig. 6. Long-term B-band light curve of HS 0728+6738 from the Wendelstein observations. The measurements span approximately 67 days. An average value of $B \sim 15.6$ is observed outside of eclipse. The large change in eclipse depth is not real but due to missing data points at mid-eclipse in many of the light curves.

We then get $i = 5.7\,\Delta V + 70.6 \simeq 86°$ for $\Delta V \sim 2.7$. This value agrees well with the estimate derived above from the eclipse profiles.

3.4. Long-term behaviour

Figure 6 shows the long-term light curve of HS 0728+6738. The apparent magnitudes of the comparison stars listed by the USNO-A2.0 catalogue were combined with the instrumental ones to obtain the (approximate) B-band magnitudes of HS 0728+6738. A mean out-of-eclipse magnitude of $B \sim 15.6$ is derived from the long-term light curve, which agrees with the USNO measurements of HS 0728+6738 itself. From our limited data, it is apparent that the out-of-eclipse level changes by ∼0.3 mag on time scales of weeks.

4. Spectroscopic analysis

4.1. The average optical spectrum

Figure 7 presents the normalised blue and red average spectra of HS 0728+6738. The emission pattern is dominated by intense, single-peaked lines of the Balmer series (from Hα to H8) and He I (like the transitions at λ4922, λ4472 and λ4026). In constrast to the Balmer lines the He I profiles are almost flat-topped, and double-peaked profiles start to develop bluewards of He I λ4472. The strength of the He II λ4686 and the Bowen blend indicates the presence of a source of ionising photons. The emission lines of HS 0728+6738 also have highly asymmetric profiles with enhanced wings extending up to ∼±2000 km s^{-1} from the line centre. Table 3 lists the equivalent widths (*EW*) and full-widths at half-maximum (*FWHM*) of the strongest lines. The *FWHM*s were obtained by fitting Gaussians to the line profiles. The red spectrum does not contain any spectral feature that could be ascribed to the photospheric emission of the companion star. The absorption line bluewards of Hε is the Ca II K line, which has an interstellar origin and an equivalent width of ∼0.2 Å.

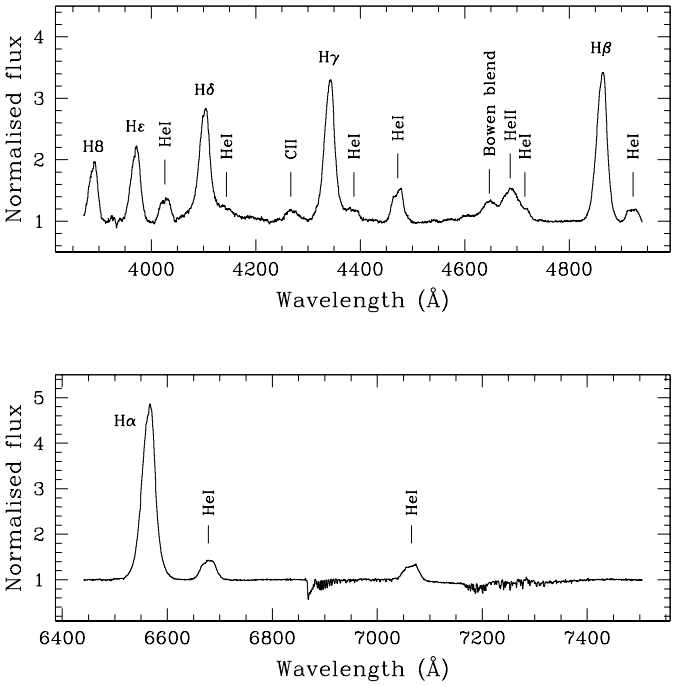

Fig. 7. Blue and red average spectra of HS 0728+6738.

Table 3. Line parameters measured from the average optical spectrum.

Line	*EW* (Å)	*FWHM* (km s^{-1})	Line	*EW* (Å)	*FWHM* (km s^{-1})
Hα	124	1340	He II λ4686	17	2680
Hβ	57	1440	Bowen blend	9	2415
Hγ	55	1625	C II λ4267	5	2090
Hδ	49	1770	He I λ6678	14	1360
Hε	27	1570	He I λ4472	12	1560
H8	19	1485	He I λ4026	8	1730

4.2. Radial velocities

In order to analyse the effect of the orbital motion on the emission lines we measured the radial velocities of Hα, Hβ, He I λ4472, and He II λ4686 by convolving the individual profiles with Gaussian templates. The convolution was performed on a window suitably selected for not including any contaminating feature. The *FWHM* of each Gaussian template was chosen as the *FWHM* of the average line profile in each case (see Table 3). The radial velocity curves obtained in this way are shown in Fig. 8. We then fitted the velocity curve of each line with a sinusoidal function of the form:

$$V_{\rm r} = \gamma - K \sin\left[2\pi\,(\varphi - \varphi_0)\right].$$

In Table 4 we list the resulting fitting parameters. The absolute values of the K and γ velocities should be treated with caution as they depend on the method of the radial velocity measurement. Repeating the analysis described above using a double Gaussian method (Schneider & Young 1980) with a Gaussian separation of 1000 km s^{-1} yields K velocities larger by a factor of two than those reported in Table 4, which agree with the high velocity line wings seen in the trailed spectra diagrams

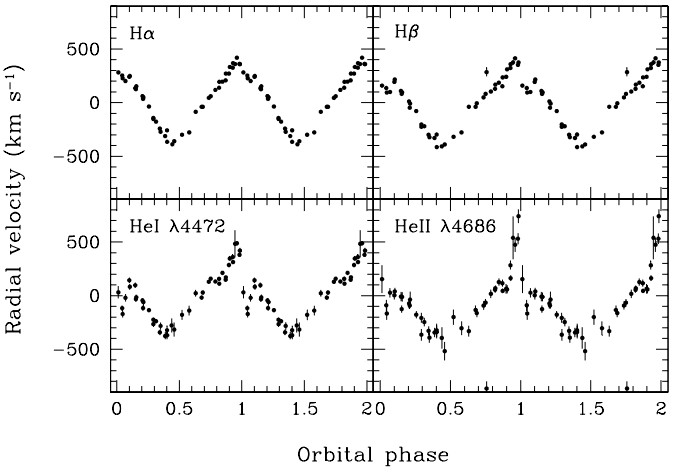

Fig. 8. Radial velocity curves of Hα, Hβ, He I λ4472, and He II λ4686 as a function of orbital phase. No phase binning has been applied and a full orbital cycle has been repeated for continuity.

Table 4. Radial velocity curve fitting parameters.

Line	γ (km s^{-1})	K (km s^{-1})	φ_0
Hα	0.8 ± 0.3	347.6 ± 0.5	0.2267 ± 0.0002
Hβ	−23.3 ± 0.8	344 ± 1	0.2152 ± 0.0005
He II λ4686	−21 ± 4	317 ± 5	0.189 ± 0.003
He I λ4472	−121 ± 7	255 ± 11	0.208 ± 0.006

(Fig. 10). The statistical errors on the velocity measurements are of the order of a few km s^{-1} for both methods.

All the radial velocity curves are delayed with respect to the assumed motion of the white dwarf by $\varphi_0 \simeq 0.2$. This phase lag indicates that the main emission site is at an angle of ∼72° to the line of centres between the centre of mass and the white dwarf. Interestingly, He II λ4686 is also delayed by approximately the same amount, indicating that the bulk of this emission is located close in azimuth to the region where Balmer and He I emission comes from.

All the radial velocity curves displayed in Fig. 8 show evidence for rotational disturbance around zero phase, suggesting that some fraction of the emission line flux originates in an accretion disc.

4.3. Equivalent width curves

We have computed the equivalent widths (*EW*s) of the Hα, Hβ, He I λ4472, and He II λ4686 emission lines in each individual spectrum. In Fig. 9 we present the resulting *EW* curves as a function of orbital phase. Hα, Hβ, and He I λ4472 show strong peaks during the eclipse, indicating that the regions responsible for the emission of these lines are eclipsed to a lesser degree than the regions emitting the continuum. This behaviour requires that the bulk of the Balmer and He I originates either far outside the Roche lobe of the primary, or situated above the orbital plane. Further support to this hypothesis is given by the fact that most of the emission lines in the far-ultraviolet (FUV) remain uneclipsed (see Fig. 11 and Sect. 4.5). Interestingly, He II λ4686 is eclipsed at a level comparable to that of the

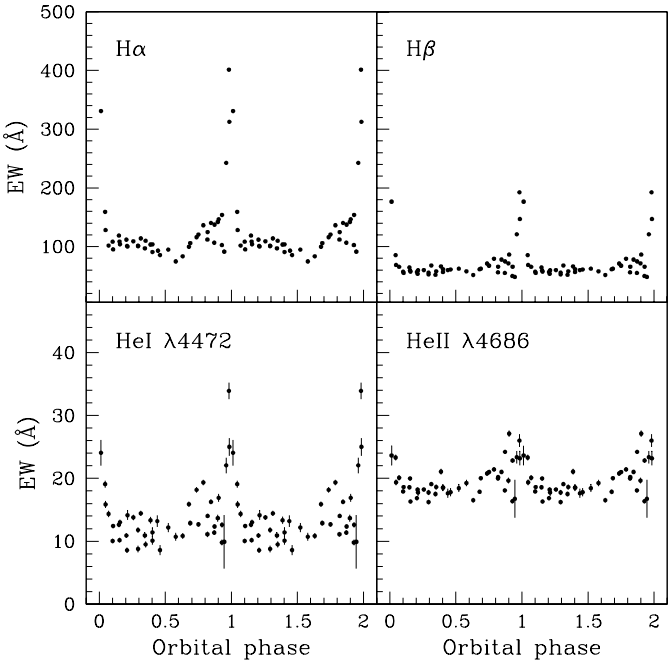

Fig. 9. Equivalent width curves of Hα, Hβ, He I λ4472, and He II λ4686 as a function of orbital phase. No phase binning has been applied and a full orbital cycle has been repeated for continuity.

continuum, consistent with the near-absence of He II λ1640 in the in-eclipse FUV spectrum (see Fig. 11 and Sect. 4.5).

4.4. Trailed spectra

Trailed spectra diagrams of the Hα, Hβ, He I λ4472, and He II λ4686 lines were constructed after rebinning the spectra on to a uniform velocity scale centred on the rest wavelength of each line. They are presented in Fig. 10. All the lines are dominated by a high-velocity emission S-wave which reaches maximum blue velocity at $\varphi \simeq 0.45$. The Balmer, He I and He II emissions reach velocities $\gtrsim$1000 km s^{-1} at $\varphi \sim 0$ and $\lesssim$−1000 km s^{-1} half an orbit later. The Balmer and He I emission S-waves are significantly absorbed at $\varphi \sim 0.5$, but little or no absorption is seen in He II λ4686.

4.5. The far-ultraviolet spectrum

Our brief *HST* observation (Sect. 2.3) has been obtained exactly during mid-eclipse ($\varphi = 0.0$). The FUV spectrum of HS 0728+6738 (Fig. 11) is completely dominated by emission lines of Lyα, C, N, and Si with extremely weak continuum flux, again indicating that the regions producing both low and high excitation emission lines are not eclipsed and are located either far outside the Roche lobe of the primary or above the orbital plane. The *EW*s of the strongest lines are given in Table 5. Several narrow lines are detected that are most probably of interstellar origin (e.g. the N I λ1200 triplet and Si II λ1304). Interstellar absorption by neutral hydrogen is also the likely cause of the dip near 1215 Å between the blue wing of Lyα and Si II λ1206. The line flux ratios of the emission lines are overall typical of normal CVs, with C IV λ1550 being the strongest line

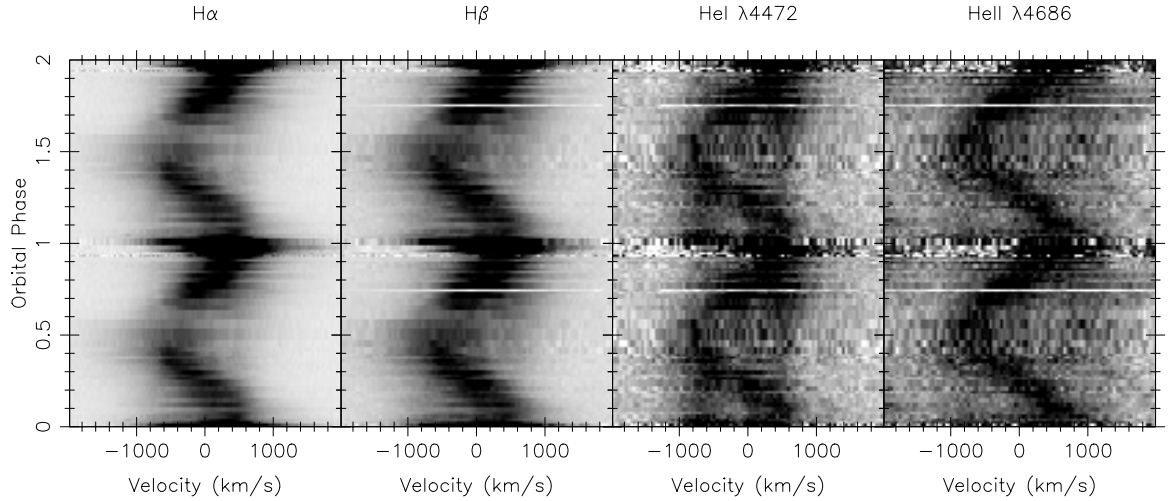

Fig. 10. Trailed spectra of Hα, Hβ, He I λ4472, and He II λ4686. No phase binning has been applied. Black represents emission and a full orbit has been repeated for clarity.

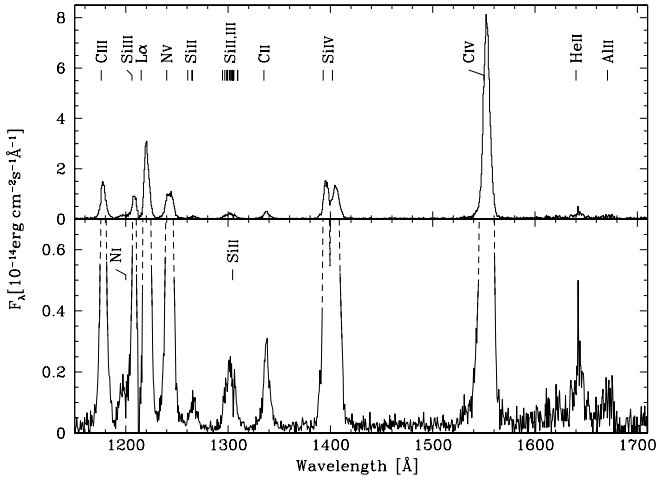

Fig. 11. *HST*/STIS far-ultraviolet spectrum of HS 0728+6738 taken at mid-eclipse. Note the absence of significant continuum flux and the strong emission lines.

and relatively weak N v λ1240 emission (see e.g. Mauche et al. 1997; Gänsicke et al. 2003). Unusual is, however, the weakness of He II λ1640, which is consistent with the fact that the optical He II λ4686 is eclipsed to a similar degree as the continuum emission (Fig. 9). Moreover, the He II λ1640 emission shows evidence for a narrow component. Our single *HST* spectrum of HS 0728+6738 suggests that part of the He II emission originates in a region different from that emitting the bulk of the FUV emission lines. Time-resolved FUV spectroscopy covering the entire eclipse would be an important probe to map the various emission regions in HS 0728+6738.

5. HS 0728+6738 as a new SW Sextantis star

We suggest that HS 0728+6738 is a genuine SW Sextantis star, and we will compare in the following sections its characteristics to those of the confirmed members of the SW Sex class.

Table 5. Equivalent widths of the emission lines contained in the *HST*/STIS spectrum of HS 0728+6738.

Line	*EW* (Å)	Line	*EW* (Å)
Lyα	190:[1]	Al II λ1670	30 ± 12
He II λ1640	30 ± 12	Si II λ1260	30 ± 8
C II λ1335	110 ± 10	Si III λ1206	32:[1]
C III λ1176	260 ± 20	Si III λ1300	160 ± 15
C IV λ1550	2000 ± 150	Si IV λ1400	1000 ± 80
N v λ1240	240 ± 20		

[1] Uncertain because of Lyα/Si III λ1206 blending and interstellar Lyα absorption.

5.1. The optical light curve

The light curve of HS 0728+6738 is very similar to those of the eclipsing SW Sex stars, such as V348 Pup (Rolfe et al. 2000), DW UMa (Shafter et al. 1988) or V1315 Aql (Dhillon et al. 1991). It exhibits V-shaped eclipses, short time-scale variations and does not show a significant pre-eclipse hump due to a conspicuous bright spot (as is the case for the majority of nova-like CVs).

The average eclipse depth observed in HS 0728+6738 is 2.7 mag, which is the deepest eclipse recorded in any SW Sex star (the previous record holder was V1315 Aql with an average eclipse depth of 1.9 mag; Dhillon et al. 1991).

5.2. Short time-scale variability in the light curve

The fast variability seen in HS 0728+6738 outside eclipse resembles the quasi-periodic oscillations (QPOs) on time scales of 10−30 min which are detected in many SW Sex stars (see Patterson et al. 2002 and references therein). Rodríguez-Gil et al. (2001a) have proposed that the SW Sex stars may contain magnetic white dwarfs whose asynchronous rotation can give rise to observable phenomenology such as short time-scale variations both in the light curves and the emission lines

(emission-line flaring), and variable circular polarisation. The accretion scenario they suggested relies on two mechanisms: stream overflow and magnetic field-stream coupling. By assuming that the overflown stream couples to the white dwarf's magnetosphere at approximately the corotation radius one gets a relationship between the orbital ($P_{\rm orb}$) and spin period (P_1) such as

$$P_1 = 0.31\, f^{3/2}\, P_{\rm orb}, \quad (5)$$

where $f \simeq 0.4$–0.6. Assuming $f \sim 0.5$, we obtain $P_1 \sim 20$ min for HS 0728+6738. If two-pole accretion is taking place, we would expect a modulation with a characteristic time scale of half the spin period, that is, ∼10 min, which is similar to the time scale of the observed oscillations in HS 0728+6738.

5.3. Spectroscopic behaviour

The optical spectrum of HS 0728+6738 is very similar to that of the deeply-eclipsing SW Sex stars, e.g. LX Ser (Young et al. 1981), BH Lyn (Dhillon et al. 1992), and V1315 Aql (Dhillon & Rutten 1995). All the SW Sex stars show single-peaked emission line profiles. At certain orbital phases, the lines exhibit central absorption structures which mimic double-peaked profiles. The strength of these absorption structures peaks around $\varphi \sim 0.5$ and increases with increasing line excitation level. Also characteristic of the SW Sex stars are the highly asymmetric line profiles. The broad wings are the result of the motion of the high-velocity S-wave. The velocity semi-amplitude of the S-wave in HS 0728+6738 is consistent with that of the S-waves seen in other eclipsing SW Sex stars.

The Balmer, He I and He II radial velocity curves are delayed by ∼0.2 orbital cycles with respect to the photometric ephemeris. This is also a defining feature of the SW Sex stars.

The *EW* curves of HS 0728+6738 reveal another key feature of the SW Sex stars: the lines are less eclipsed than the continuum, suggesting an origin either outside the Roche lobe of the primary or above the main continuum source, i.e. the disc.

The trailed spectra show an emission-line behaviour very similar to that of the deeply-eclipsing SW Sex stars BH Lyn (Hoard & Szkody 1997), BT Mon (Smith et al. 1998), and V348 Pup (Rodríguez-Gil et al. 2001b), with the exception that He II λ4686 is not dominated by the high-velocity S-wave in these three objects.

6. Conclusions

In the course of this paper we have provided sufficient evidence to classify HS 0728+6738 as a new eclipsing SW Sex star. The observed behaviour matches all the conditions needed to be a member of this class of CVs, namely:

1. The optical spectrum of HS 0728+6738 is dominated by strong, single-peaked Balmer, He I and He II emission lines. Intense, single-peaked lines are also observed in the FUV.
2. The *EW* curves reveal that the emission lines are less obscured than the continuum during eclipse. The mid-eclipse FUV spectrum shows almost no continuum but strong emission lines remain, supporting the hypothesis of the presence of a line-emitting site above the disc.
3. Line emission is dominated by an intense, high-velocity S-wave reaching velocities of $\sim\pm1000$ km s^{-1}. The S-wave reaches bluest velocity at $\varphi \sim 0.45$, a well-known characteristic of the emission S-waves in the rest of the SW Sex stars.
4. The radial velocities of the Balmer, He I, and He II lines show the characteristic ∼0.2-cycle phase delay with respect to the motion of the primary.
5. The Balmer and He I S-waves show absorption at $\varphi \sim 0.5$.
6. The optical light curve displays variations at a time scale of ∼7 min. It is now accepted that most of the SW Sex stars exhibit QPOs in their light curves (see Patterson et al. 2002, and references therein), and HS 0728+6738 does not seem to be an exception.

Acknowledgements. We thank the anonymous referee for his/her valuable comments on the original manuscript. We are grateful to Otto Bärnbanter and Christoph Ries for carrying out the Wendelstein observations. P.R.G. and B.T.G. thank PPARC for support through a PDRA and an AF, respectively. The HQS was supported by the Deutsche Forschungsgemeinschaft through grants Re 353/11 and Re 353/22. The use of the MOLLY package developed and maintained by Tom Marsh is acknowledged.

References

Araujo-Betancor, S., Gänsicke, B. T., Hagen, H.-J., Rodríguez-Gil, P., & Engels, D. 2003, A&A, 406, 213
Bertin, E., & Arnouts, S. 1996, A&AS, 117, 393
Dhillon, V. S., Jones, D. H. P., Marsh, T. R., & Smith, R. C. 1992, MNRAS, 258, 225
Dhillon, V. S., Marsh, T. R., & Jones, D. H. P. 1991, MNRAS, 252, 342
Dhillon, V. S., & Rutten, R. G. M. 1995, MNRAS, 277, 777
Eggleton, P. P. 1983, ApJ, 268, 368
Gänsicke, B. T., Araujo-Betancor, S., Hagen, H.-J., et al. 2004, A&A, 418, 265
Gänsicke, B. T., Szkody, P., de Martino, D., et al. 2003, ApJ, 594, 443
Gänsicke, B. T. 1997, Ph.D. Thesis, Universität Göttingen
Gänsicke, B. T., Fried, R. E., Hagen, H.-J., et al. 2000, A&A, 356, L79
Gänsicke, B. T., Beuermann, K., & Reinsch, K. 2002a, The physics of cataclysmic variables and related objects, ASP Conf. Ser., 261
Gänsicke, B. T., Hagen, H. J., & Engels, D. 2002b, in The physics of cataclysmic variables and related objects, ed. B. T. Gänsicke, K. Beuermann, & K. Reinsch, ASP Conf. Ser., 261, 190
Gänsicke, B. T., Hagen, H.-J., Kube, J., et al. 2002c, in The physics of cataclysmic variables and related objects, ed. B. T. Gänsicke, K. Beuermann, & K. Reinsch, ASP Conf. Ser., 261, 623
Green, R. F., Schmidt, M., & Liebert, J. 1986, ApJS, 61, 305
Groot, P. J., Rutten, R. G. M., & van Paradijs, J. 2004, A&A, 417, 283
Hameury, J. M., & Lasota, J. P. 2002, A&A, 394, 231
Hoard, D. W., & Szkody, P. 1997, ApJ, 481, 433
Horne, K. 1986, PASP, 98, 609
Hynes, R. I., Charles, P. A., Haswell, C. A., et al. 2001, MNRAS, 324, 180
Mauche, C. W., Lee, Y. P., & Kallman, T. R. 1997, ApJ, 477, 832
Nogami, D., Engels, D., Gänsicke, B. T., et al. 2000, A&A, 364, 701
Patterson, J., Fenton, W. H., Thorstensen, J. R., et al. 2002, PASP, 114, 1364
Rodríguez-Gil, P. 2003, Ph.D. Thesis

Rodríguez-Gil, P., Casares, J., Dhillon, V. S., & Martínez-Pais, I. G. 2000, A&A, 355, 181
Rodríguez-Gil, P., Casares, J., & Martínez-Pais, I. G. 2004, MNRAS, submitted
Rodríguez-Gil, P., Casares, J., Martínez-Pais, I. G., Hakala, P., & Steeghs, D. 2001a, ApJ, 548, L49
Rodríguez-Gil, P., Martínez-Pais, I. G., Casares, J., Villada, M., & van Zyl, L. 2001b, MNRAS, 328, 903
Rolfe, D. J., Haswell, C. A., & Patterson, J. 2000, MNRAS, 317, 759
Roth, M. M. 1992, in CCDs in Astronomy, ed. G. Jacoby, ASP Conf. Ser., 8, 380
Scargle, J. D. 1982, ApJ, 263, 835
Schneider, D. P., & Young, P. 1980, ApJ, 238, 946
Shafter, A. W., Hessman, F. V., & Zhang, E.-H. 1988, ApJ, 327, 248
Smith, D. A., & Dhillon, V. S. 1998, MNRAS, 301, 767
Smith, D. A., Dhillon, V. S., & Marsh, T. R. 1998, MNRAS, 296, 465
Szkody, P., Gänsicke, B., Fried, R. E., Heber, U., & Erb, D. K. 2001, PASP, 113, 1215
Thorstensen, J. R., Ringwald, F. A., Wade, R. A., Schmidt, G. D., & Norsworthy, J. E. 1991, AJ, 102, 272
Warner, B. 1995, Cataclysmic variable stars (Cambridge: Cambridge University Press)
Young, P., Schneider, D. P., & Shectman, S. A. 1981, ApJ, 244, 259